# Influence of Temperature and Pressure on the Densification, Microstructure, and Electrical Properties of the Dual-Phase System $Y_2O_3$-Doped $ZrO_2$ and $RuO_2$

Tomas P. Raming, Werner E. van Zyl,* and Henk Verweij†

*Laboratory for Inorganic Materials Science, Faculty of Chemical Technology and MESA+ Research Institute, University of Twente, P.O. Box 217, 7500 AE Enschede, The Netherlands*

*Received October 5, 2000. Revised Manuscript Received November 17, 2000*

Dual-phase nanocomposite powders of 3Y-TZP (tetragonal-$ZrO_2$ doped with 3 mol % $Y_2O_3$) and $RuO_2$ have been prepared and densified into compacts. The electrical conductivity of the densified compacts was correlated with the microstructure. Variations in the synthesis method and powder composition influenced the densification and resulting microstructure of the composites. Densification of the composites was sensitive to changes in experimental temperature/pressure conditions. Sinterforging the material in the range 1150−1250 °C and 50−100 MPa pressure resulted in dense (>95%) composites. The microstructure of the sinterforged materials revealed that macroscopic phase separation had occurred as a result of the aerial oxidation of $RuO_2$ species above ≈700 °C. Because of the volatilization of $RuO_2$, the pores in the pressed powder compact became filled with large ruthenia grains during densification. The microstructure thus reflected the agglomerate structure of the starting powder. The "inhomogeneous" microstructure led to high electrical conductivity in the material. The electrical conductivity of the dense composites was measured by the four-point technique and conductivity values on the order of $1-6 \times 10^3$ S cm$^{-1}$ were obtained. High electrical conductivity ($4.4 \times 10^3$ S cm$^{-1}$) could be obtained, even at relatively low $RuO_2$ contents of 15 mol %.

## Introduction

Ruthenia is one of the few transition-metal oxides that exhibits metallic conduction.[1] Single crystals of anhydrous $RuO_2$ have electron conductivity on the order of $2 \times 10^4$ S cm$^{-1}$ at 300 K, which along with its chemical and thermal stability, makes the material feasible for durable high-density electronic applications in the presence of water and oxygen.[2] Its use as an active electrocatalyst in anodic reactions such as $Cl_2$ or $O_2$ formation and its role in the cathodic reduction of $O_2$ have been exploited for many years.[3−7]

A serious drawback in the processing of pure $RuO_2$ powders is the well-established chemical reactivity above ≈700 °C where $RuO_2$ becomes volatile and oxidizes to $RuO_3/RuO_4$ gases (in air) or reduces to Ru metal (in a vacuum).[8] The advantage of adding a second oxidic phase such as $ZrO_2$ is not only to reduce costs but also to provide substantial stabilization of the $RuO_2$ phase against oxidation or reduction processes:

$$RuO_2 + O_2 \rightarrow RuO_4(g)$$

$$2RuO_2 + O_2 \rightarrow 2RuO_3(g)$$

$$RuO_2 \rightarrow Ru(s) + O_2\ (vacuum)$$

Provided a percolation path for electrons remains accessible, even large additions of a second phase do not necessarily impede electron conductivity. For example, up to 85 mol % of insulating $TiO_2$ has been added to $RuO_2$ without loss of electron conduction of the resulting composite.[9,10]

Electrodes based on ruthenia, or composites thereof, are usually applied as layered materials. Both wet-chemical and vapor-phase techniques have been used to deposit $RuO_2$-based electrode layers. Wet-chemical techniques include painting of a $RuCl_3$ solution onto the substrate,[11] spin coating,[12] dipping,[13−15] and electrosyn-

* To whom correspondence should be addressed.
† Present address: Department of Materials Science and Engineering, The Ohio State University, Columbus, OH 43210-1178.

(1) Goodenough, J. B. *Prog. Solid State Chem.* **1971**, *5*, 145.
(2) Schafer, H.; Schneidereit, G.; Gerhardt, W. *Z. Anorg. Allg. Chem.* **1963**, *319*, 372. (b) Trasatti G.; Lodi, G. *Electrodes of Conductive Metallic Oxides*; Elsevier: Amsterdam, 1981; part B, Chapter 10. (c) Trasatti, S.; Kurzwel; P. *Plat. Met. Rev.* **1994**, *38*, 46.
(3) Bandi, A.; Vartires, I.; Mihelis, A.; Hainarosie, C. *J. Electroanal. Soc.* **1983**, *157*, 241.
(4) Kuhn, A. T.; Mortimer, C. S. *J. Electrochem. Soc.* **1973**, *120*, 231.
(5) de Nora, O. *Chem. Eng. Technol.* **1970**, *42*, 222.
(6) Bandi, A.; Mihelis, A.; Vartires, I.; Ciortan, E.; Rosu, I. *J. Elektrochem. Soc.* **1987**, *134*, 1982.
(7) Ogura, K.; Takagi, M. *Solar Energy* **1986**, *37*, 41.
(8) Tagirov, V. K.; Chizhikov, D. M.; Kazenas, E. K.; Shubochkin, L. K. *Russ. J. Inorg. Chem.* **1975**, *20*, 1133.
(9) Trasatti, S. *Electrochim. Acta* **1991**, *36*, 225.
(10) Gerrard, W. A.; Steele, B. C. H. *J. Appl. Electrochem.* **1978**, *8*, 417.
(11) Hine, F.; Yasuda, M.; Yoshida, T. *J. Electrochem. Soc.* **1977**, *4*, 500.
(12) Guglielmi, M.; Colombo, P.; Rigato, V.; Battaglin, G.; Boscolo-Boscoletto, A.; DeBattisti, A. *J. Electrochem. Soc.* **1992**, *139*, 1655.
(13) Kameyama, K.; Tsukada, K.; Yahikozawa, K.; Takasu, Y. *J. Electrochem. Soc.* **1994**, *141*, 643.
(14) Kameyama, K.; Tsukada, K.; Yahikozawa, K.; Takasu, Y. *J. Electrochem. Soc.* **1993**, *140*, 966.

10.1021/cm001188o CCC: $20.00 
Published on Web 01/26/2001

thesis.[16] Vapor-phase techniques that have been used include MOCVD,[17,18] reactive microwave sputtering,[17] pulsed laser deposition,[19] and oxygen-plasma-assisted molecular beam epitaxy.[20]

The efficiency of electron conduction in an electrode depends largely on the generated microstructure.[10] The parameters that constitute the microstructure (grain sizes, grain morphology, porosity/pore sizes, composition, distribution, etc.) are determined by the synthesis approach and the thermal treatment given to the electrode. The influence of morphology on the properties of ruthenia-containing electrodes has often been neglected, especially in bulk composites where there is no influence of a substrate (such as in two-dimensional films) on the morphology.

In the present study, 3Y-TZP, an oxygen ion-conducting material,[21] was chosen as the second and stabilizing oxidic phase. Zirconia was previously mixed with $RuO_2$ to improve the stability of the latter as a dimensionally stable electrode.[22,23] A porous electrode material prepared from a 3Y-TZP−$RuO_2$ composite has also been evaluated for solid oxide fuel cell (SOFC) applications.[24]

All dual-phase $RuO_2$ composites reported to date were either porous gels[25−29] or porous layered electrodes.[22,23,30] Despite several attempts to densify zirconia−ruthenia[24,25,27] and zirconia−titania[31] dual-phase composites, a dense, fully crystalline $RuO_2$ composite has not been reported to date, which places restrictions on perceived applications.

## Experimental Section

**Powder Synthesis.** Two different wet-chemical synthesis routes have been used, yielding a total of four powders with different compositions. Three powders were prepared through a *coprecipitation* (CP*X*) method, where *X* denotes the molar percentage of $RuO_2$ present (determined by XRF) in the powders. An aqueous solution of $ZrOCl_2 \cdot 8H_2O$, $YCl_3$, and $RuCl_3 \cdot 3.4H_2O$ was slowly added to aqueous ammonia (pH > 13) with vigorous stirring. One powder was prepared through a *sequential precipitation* (SP*X*) method. With the SP method, $ZrO_2$ was first formed from a hydrothermal synthesis method.[32] The resulting nanocrystalline $ZrO_2$ suspension was then dispersed in aqueous ammonia (pH >13) with vigorous stirring. An aqueous solution of $RuCl_3$ was slowly added to the suspension. For both the SP and CP methods, the resulting gel precipitate was filtered, washed with water to remove chlorides and other water-soluble species, and subsequently washed with ethanol to displace the water. After the ethanolic suspension was dried at 100 °C, the resulting powders were mortared and calcined in air at 600 °C for 2 h at a heating rate of 2 °C $min^{-1}$. A detailed account of the powder synthesis and characterization has been described elsewhere.[33]

**Densification of Powders.** Organic binder (5 wt % of polyvinylpyrolidone) was mixed with the powder to obtain initial structural integrity with pressing. Compacts were formed through isostatic prepressing (200 MPa) in a flexible tube mould. The mould was removed and final pressing (400 MPa) was performed in a thin latex sheath. The binder was subsequently removed by heating at 400 °C for 1 h at a heating rate of 0.5 °C $min^{-1}$. One compact was sintered pressureless by heating at 1150 °C for 2 h with a heating rate of 2 °C $min^{-1}$. All compacts for sinterforging were presintered through heating at 2 °C $min^{-1}$ to 800 °C, kept at this temperature for 2 h, and then cooled to room temperature. The resulting compacts (≈1 $cm^3$ in size) were placed between two SiC pistons and sinterforged using a standard heat program for each compact. Heating started from room temperature at a rate of 10 °C $min^{-1}$ until 800 °C was reached and then a rate of 2 °C $min^{-1}$ up to 50 °C below the set temperature (either 1150 or 1250 °C) before the sinterforge part of the program started. Heating continued at 2 °C $min^{-1}$ until the set temperature was reached while simultaneously increasing the pressure to either 50 or 100 MPa. The temperature and pressure were kept constant for 25 min, after which the pressure was released and the sample cooled until ambient conditions were reached.

**Characterization.** The composition of the powders and compacts was determined with quantitative X-ray fluorescence spectrometry (XRF) using a Philips PW 1480/10 fluorometer (Eindhoven, The Netherlands). The XRF measurement method was described previously.[34] The phase composition of the compacts was investigated with a Philips X'Pert-1 PW3710 X-ray diffractometer (Eindhoven, The Netherlands) using Cu Kα radiation. The divergence slit was set to either 1° using a Ni filter in the secondary (diffracted) beam or to an irradiated length of 10 mm when using a secondary curved graphite monochromator optimized for Cu radiation. The receiving slit was set to 0.1 mm in all cases. The density of the compacts was determined with the Archimedes method using the liquid mercury for nondense (<90%) and water for dense (>90%) compacts.

The compacts were investigated with scanning electron microscopy (SEM) coupled with an energy-dispersive X-ray microanalysis system (EDAX-mapping). A Philips XL30 ESEM-FEG (environmental scanning electron microscope with field emission gun) was utilized to obtain BSE (backscatter electron) micrographs at different magnifications. The SEM was coupled with an EDAX DX4 (Mahwah, New Jersey) system that was used to generate electron maps using Mn Kα radiation at 132-eV resolution.

The electrical conductivity was measured with a Matheson conductive probe consisting of four point needles. The four needles were aligned in a linear configuration at a distance of 1.5 mm apart. The samples were thin square rods, sliced from the sintered compacts, with diameter 0.4−0.5 mm and a length of at least 6 mm. The high axial ratio is necessary to obtain an electric field in the material with approximately straight electric field lines.

(15) Ito, M.; Murakami, Y.; Kaji, H.; Yahikozawa, K.; Takasu, Y. *J. Electrochem. Soc.* **1996**, *143*, 32.
(16) Zhitomirsky, I.; Gar-Or, L. *Mater. Lett.* **1997**, *31*, 155.
(17) Huang, Y. S.; Liao, P. C. *Sol. Eng. Mater. Solid Cells* **1998**, *55*, 179.
(18) Park, S.-E.; Kim, H.-M.; Kim, K.-B.; Min, S.-H. *J. Electrochem. Soc.* **2000**, *147*, 203.
(19) Jia, Q. X.; Arendt, P.; Groves, J. R.; Fan, Y.; Roper, J. M.; Foltyn, S. R. *J. Mater. Res.* **1998**, *13*, 2461.
(20) Gao, Y.; Bai, G.; Liang, Y.; Dunham, G. C.; Chambers, S. A. *J. Mater. Res.* **1977**, *12*, 1844.
(21) Jiang, S.; Schulze, W. A.; Amarakoon, V. R. W.; Stangle, G. C. *J. Mater. Res.* **1997**, *12*, 2374.
(22) Camara, O. R.; Trasatti, S. *Electrochim. Acta* **1996**, *41*, 419.
(23) Burke, L. D.; McCarthy, M. *Electrochim. Acta* **1984**, *29*, 211.
(24) Hrovat, M.; Holc, J.; Kolar, D. *Solid State Ionics* **1994**, *68*, 99.
(25) Colomer, M. T.; Jurado, J. R. *J. Solid State Chem.* **1998**, *141*, 282. (b) Ryan, J. V.; Berry, A. D.; Anderson, M. L.; Long, J. W.; Stroud, R. M.; Cepak, V. M.; Browning, V. M.; Rolison, D. R.; Merzbacher, C. I. *Nature* **2000**, *406*, 169.
(26) Colomer, M. T.; Jurado, J. R. *J. Non-Cryst. Sol.* **1997**, *217*, 48.
(27) Djurado, E.; Roux, C.; Hammou, A. *J. Eur. Ceram. Soc.* **1996**, *16*, 767.
(28) Hammou, A.; Djurado, E.; Roux, C.; Micheau, C. *Proc. Electrochem. Soc.* **1993**, *93−4*, 48.
(29) Long, Y. C.; Zhang, Z. D.; Dwight, K.; Wold, A. *Mater. Res. Bull.* **1988**, *23*, 631.
(30) Hrovat, M.; Bernik, S.; Holc, J. *J. Mater. Sci. Lett.* **1999**, *18*, 1019.
(31) Colomer, M. T.; Jurado, J. R. *Chem. Mater.* **2000**, *12*, 923.
(32) Sagel-Ransijn, C. D.; Winnubst, A. J. A.; Burggraaf, A. J.; Verweij, H. *J. Eur. Ceram. Soc.* **1996**, *16*, 759.
(33) Raming, T. P. Ph.D. Thesis, University of Twente, Enschede, The Netherlands, 2000.
(34) Bos, J. A. M.; Vrielink, L.; van der Linden, W. E. *Anal. Chim. Acta* **2000**, *412*, 203.

**Table 1. Quantitative XRF Data Showing the Molar Composition of the System $Y_2O_3$-Doped-$ZrO_2$ and $RuO_2$ Nanocomposite Powders after Calcination at 600 °C**

| powder | $ZrO_2$, mol % | $Y_2O_3$, mol % | $HfO_2$, mol % | $RuO_2$, mol % | Cl, mol % |
|---|---|---|---|---|---|
| CP46 | 49.7 | 3.1 | 0.5 | 46.3 | 0.1 |
| SP35 | 61.4 | 2.7 | 0.6 | 34.8 | 0.4 |
| CP33 | 63.0 | 3.2 | 0.6 | 33.0 | 0.2 |
| CP15 | 79.4 | 4.1 | 1.0 | 15.1 | 0.4 |

**Table 2. Relative Density (%) of Compacts from Different Densification Methods: SF = Sinterforging; PS = Pressureless Sintering**

| sintering method | PS | SF | SF | SF | SF |
|---|---|---|---|---|---|
| temperature (°C) | 1150 | 1000 | 1150 | 1150 | 1250 |
| pressure (MPa) | 0 | 100 | 100 | 50 | 50 |
| | Relative Density (%) | | | | |
| CP46 | | | 89.7 | 82.9 | 97.9 |
| SP35 | | | 93.5 | 89.9 | |
| CP33 | 58.2 | 69.5 | 95.7 | 93.8 | 96.6 |
| CP15 | | | 98.1 | 96.8 | |
| 3Y-TZP | 97.3 | | | | |

## Results and Discussion

**Composition and Densification.** The molar compositions of the powders, calcined at 600 °C, have been determined by quantitative XRF. The $RuO_2$ content was varied in the range 15−46 mol %. The results are shown in Table 1.

The green densities of the pressed compacts (presintered) were all in the range 48−53%. The densities obtained from both pressureless sintering and sinterforging are shown in Table 2.

Sintering without added pressure at 1150 °C or sinterforging at 1000 °C at 100 MPa did not lead to a dense compact for CP33 from which we concluded that the presence of $RuO_2$ impeded densification through sintering in this system. A pure 3Y-TZP compact, for example, could be densified to >97% by pressureless sintering at 1150 °C. For each pressure used during sinterforging, the relative density of all composites decreased with increasing $RuO_2$ content. This conclusion is also in accordance with results obtained for the $TiO_2$−$RuO_2$ composite system,[31] where densities (after sintering at 1300 °C) decreased from 85 to 73% while the $RuO_2$ content increased from 5 to 50 mol %, respectively. Higher sinterforge pressures led to higher densities at 1150 °C. Dense composites (>95%) for both CP33 and CP15 were obtained after sinterforging at 1150 °C with 100 MPa pressure. The composite CP46 was densified to almost 98% density by increasing the sinterforge temperature to 1250 °C while keeping the pressure relatively low at 50 MPa, indicating the sensitivity of the system to temperature/pressure changes during sinterforging.

**Composition and Microstructure of Sintered Compacts.** Sintering of $RuO_2$ composites previously led to partial[31] or even complete loss of the $RuO_2$ phase.[27,28] Oxidation reactions and subsequent sublimation processes of $RuO_2$ in the composite are composition- and temperature-dependent. At a low $RuO_2$ content (<10 mol %), the $RuO_2$ was reported to be retained inside the composite up to a temperature of 1300 °C, but at higher $RuO_2$ content,[31] or higher temperature,[22] the $RuO_2$ was partially oxidized and sublimed out of the compact.

The $RuO_2$ content of several sintered samples was measured with quantitative XRF. The surfaces of the samples that were sintered at temperatures above 1000 °C were gray-white, suggesting the outer surface became zirconia-rich and ruthenia-poor as a result of the sublimation of the latter. The Ru contents of both the outer surface layer and the bulk of the materials were determined. The information depth for quantitative XRF of these samples was ≈100 $\mu$m. The compacts that were sinterforged at 1150 °C did not show (by XRF) noticeable loss of $RuO_2$, implying that loss of $RuO_2$ only occurred from a depth of a few micrometers. The compacts that were sinterforged at 1250 °C showed a concentration gradient for $RuO_2$ in the material. The outer layer (≈100 $\mu$m) showed a loss of 8−10 mol % of $RuO_2$, while the bulk had lost 3−5 mol % of the total amount of $RuO_2$ present in the CP33 and CP46 compacts. The CP46 compact showed a higher loss (5 mol %) compared to the CP33 compact (3 mol %). Significant loss of $RuO_2$ from the composites investigated in this study thus starts between 1150 and 1250 °C during sinterforging. Rapid densification due to the applied pressure during sinterforging prevents large-scale loss of $RuO_2$ from the compacts at ≤1150 °C. X-ray diffraction patterns showed the presence of tetragonal-$ZrO_2$ and $RuO_2$ as the exclusive phases identified for all composites both before and after sintering.

**Microstructure of the Sintered Compacts.** The microstructure of CP33 sinterforged at 1150 °C under 100 MPa is shown in Figure 1. Segregation between the $ZrO_2$ and $RuO_2$ phases has occurred macroscopically.

Ruthenia grains present near surfaces sublimed into the pore spaces and subsequently condensed during the closure of the pores. The peripheries of the agglomerates in the compacts were therefore leached from the $RuO_2$ phase and consisted of pure $ZrO_2$, while the pores between the agglomerates were filled with $RuO_2$. In the mid-region of the original agglomerates a homogeneous distribution of small (below 200 nm) $RuO_2$ and $ZrO_2$ grains remained, as shown in Figure 2.

The phase distribution and microstructure shown in Figure 1 closely resembles the phase distribution and microstructure reported by Hammou et al.[28] for porous $ZrO_2$−$RuO_2$ composites that were sintered pressureless at 900 °C. In that study the agglomerate boundaries were also enriched with ruthenia.

The microstructure of CP46, sinterforged at 1150 °C and 100 MPa pressure, closely resemble the microstructure of the CP33 compact after sinterforging. The major difference between CP33 and CP46 was the greater number of pores present in the latter compact, also reflected in the lower measured density (see Table 2). Apart from an increase (factor of 1.5−2) of $RuO_2$ bulk grain sizes due to the higher sinterforging temperature, the microstructures of the CP33 and CP46 compacts that were sinterforged at 1250 °C appeared similar to the compacts sinterforged at 1150 °C.

The microstructure of CP15 sinterforged at 1150 °C and 100 MPa pressure also showed macroscopic phase separation between the zirconia and the ruthenia phases as shown in Figure 3. There was, however, a distinct difference between the CP15 microstructure when compared to CP33 and CP46. In the former phase segregation was “complete” while in the latter two only “partial”. In the composite CP15, ruthenia that was originally present both at the peripheries and interior

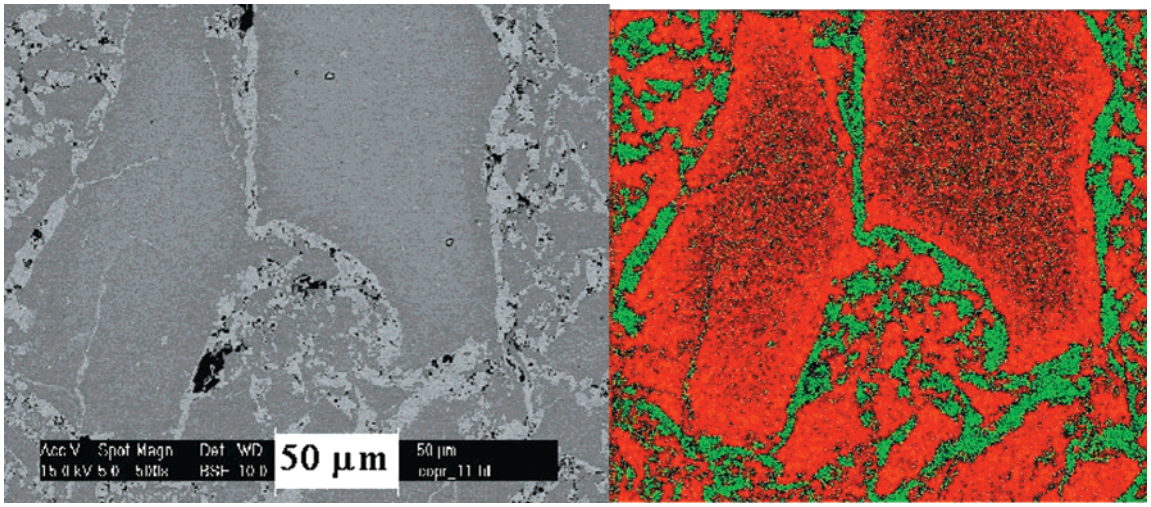


**Figure 1.** Backscatter electron-SEM micrograph (left) and electron mapping (EDAX) of the same area in the CP33 composite sinterforged at 1150 °C and 100 MPa pressure. Key: green = $RuO_2$; red = $ZrO_2$.

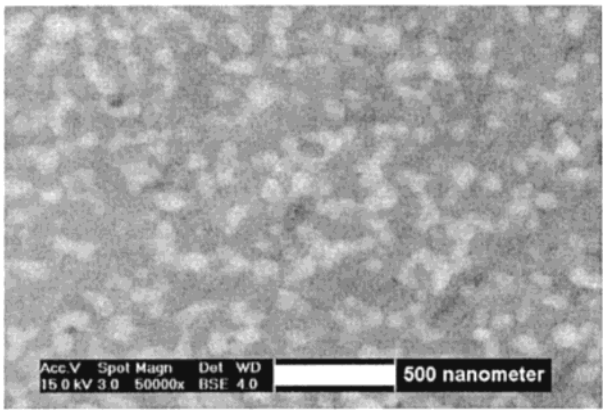


**Figure 2.** Backscatter electron-SEM micrograph of the mid-region of the agglomerates in the CP33 composite sinterforged at 1150 °C and 100 MPa pressure. Light phase = $RuO_2$; dark phase = $ZrO_2$.

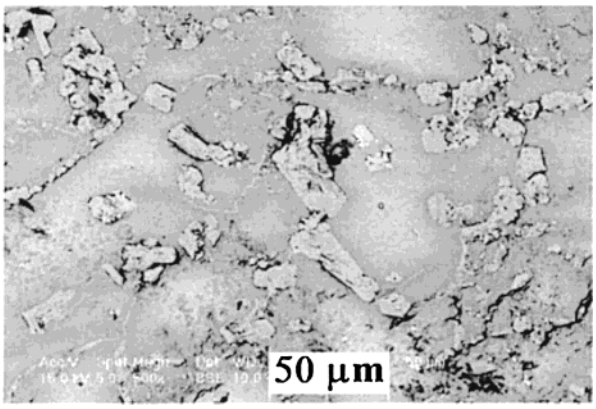


**Figure 3.** Backscatter electron-SEM micrograph of CP15 composite sinterforged at 1150 °C and 100 MPa pressure.

of the agglomerates had been re-deposited inside the pores, while in the other two cases only the ruthenia at the periphery of the agglomerates deposited inside the pores.

The compact obtained from the sequential precipitation, SP35, sinterforged at 1150 °C and 100 MPa pressure also showed macroscopic phase segregation, but in a different manner compared to the CP-prepared composites. The microstructure was very irregular, as can be seen in Figure 4, and did not show as many remnants of the original agglomerates as did the CP-type compacts. Areas with both very large (up to 10 $\mu$m) and relatively small (below 1 $\mu$m) $RuO_2$ grains could be discerned. The final microstructure of the 3Y-TZP and $RuO_2$ composites was therefore influenced not only by the $RuO_2$ oxidation process but also by the phase distribution in the powder. The SP powder had a less homogeneous distribution of phases after calcination compared to the CP powders[33] but after sintering showed less phase segregation than the CP powders. In summary, macroscopic phase separation occurred in all composites after sinterforging. From the resulting microstructures three main areas could be discerned, namely, (i) a "homogeneous" area in the center of the agglomerates where $ZrO_2$ and $RuO_2$ phases are equally distributed (see Figure 2), (ii) a $RuO_2$ area between the agglomerates, and (iii) a $ZrO_2$ area at the periphery of the bulk agglomerates.

**Electrical Conductivity.** The electrical conductivity of pure single-crystalline ruthenia is $2.5 \times 10^4$ S cm$^{-1}$.[18] On the basis of the high electrical conductivity measured, a percolative electron conductive pathway was operative in all composites (see Table 3). The CP33 compacts sinterforged at either 1150 or 1250 °C had the highest electrical conductivity at $6.7 \times 10^3$ S cm$^{-1}$. The conductivity of CP46 sinterforged at 1150 °C was slightly lower.

The microstructures of the composites contain large $RuO_2$ grains that provided excellent electron conduction pathways. The $RuO_2$ grains that were concentrated between the agglomerates are believed to be mainly responsible for the electron conduction because they appear to form a continuous pathway. The electrical conductivity measured for the CP33 compacts sinterforged at either 1150 and 1250 °C were similar and indicated that the microstructure did not disrupt the electrical properties when heating from 1150 to 1250 °C, as verified by the SEM investigation also.

The electrical conductivity of CP15 sinterforged at 1150 °C was a factor of 1.5 lower compared to those of the CP33 and CP46 compacts. Because all $RuO_2$ was present in large $RuO_2$ grains around the agglomerates (in contrast to CP33 and CP46), more $RuO_2$ grains were

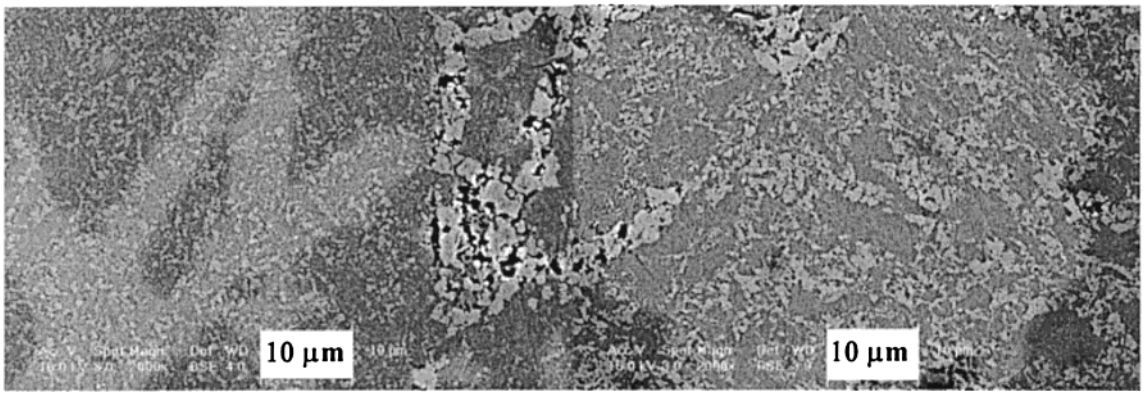


**Figure 4.** Backscatter electron-SEM micrograph of SP35 composite sinterforged at 1150 °C and 100 MPa pressure.

**Table 3. Electrical Conductivity (Siemens per Centimeter) of Composites Sinterforged at Different Temperatures and Pressures[a]**

| sintering method | PS | SF | SF | SF |
|---|---|---|---|---|
| temperature °C) | 1150 | 1000 | 1150 | 1250 |
| pressure (MPa) | 0 | 100 | 50 | 50 |
| | Electrical Conductivity (S $cm^{-1}$) | | | |
| CP46 | | | $6.3 \times 10^3$ | |
| SP35 | | | $1.0 \times 10^3$ | |
| CP33 | $4.8 \times 10^3$ | $4.3 \times 10^3$ | $6.7 \times 10^3$ | $6.7 \times 10^3$ |
| CP15 | | | $4.4 \times 10^3$ | |

[a] Pure $RuO_2$ (ref 2); 25 at 300 K.

available for electron conduction and hence a relatively high conductivity was obtained with respect to the total amount of $RuO_2$ present.

Because the CP15 compact showed metallic conduction, the percolation limit for this system (due to its inhomogeneous phase distribution) is equal or lower than 15 mol % $RuO_2$. Such a low percolation limit has not been previously observed for any $RuO_2$-containing composite. The comparable zirconia−ruthenia system[28] prepared by pressureless sintering at 900 °C showed the percolation limit was at least 20 mol % $RuO_2$ because that was the upper limit of the $RuO_2$ composition in the composite, yet no electrical conductivity was found because it was not a dense compact. In that study it was demonstrated that, despite a sufficient $RuO_2$ content, the low sintering temperature resulted in low-density compacts, which was not sufficient for developing significant phase segregation and subsequently for creating a percolative $RuO_2$ phase in the material. The percolation limit for a two-phase titania ruthenia composite, sintered at 1300 °C, was found to be ≈26 mol % $RuO_2$.[31] These compacts also showed an inhomogeneous distribution of the two phases and had a density of 70−80%, which probably contributed to an increase in the percolation limit. The SP35 compact that was sinterforged at 1150 °C had an electrical conductance 7 times lower than that of the CP33 compact. The phase segregation in SP35, as discussed, resulted in a different type of phase distribution in the microstructure when compared to that of the CP-type composites. The $RuO_2$ grains of the SP35 compact show less connectivity of the grains compared to those of the CP compacts, as could also be inferred from the SEM micrographs. This difference in electron conductivity between the SP and CP compacts demonstrates the influence of the synthesis method and subsequent microstructure on the electrical properties of these materials.

## Conclusions

Dense (>95%) dual-phase composites consisting of 3Y-TZP and $RuO_2$ phases were obtained through sinterforging at 1150 °C/100 MPa or 1250 °C/50 MPa. In the former no significant loss of $RuO_2$ from the composites were detected; in the latter the maximal loss was 5 mol %. Pressureless sintering at 1150 °C led to compacts with low density (below 70%). The presence of $RuO_2$ in the composites impeded densification when compared to a pure, 3Y-TZP compact after sintering. The higher the $RuO_2$ content, the lower the final density obtained using similar experimental conditions. Sintering the zirconia−ruthenia compacts at 1000 °C or higher temperature led to macroscopic phase segregation. The ruthenia at the peripheries of the agglomerates sublimed as $RuO_4$ (g) into the pores where it condensed, forming micrometers thick and tens of micrometers long ruthenia-enriched areas. In the mid-region of the agglomerates, a homogeneous mixture of zirconia and ruthenia grains smaller than 200 nm was retained. At low $RuO_2$ percentage (15 mol %) all $RuO_2$ was redeposited inside the pores upon sinterforging at 1150 °C/100 MPa, forming micrometer-sized ruthenia grains with no small ruthenia grains left in the bulk.

All 3Y-TZP−$RuO_2$ compacts in this study were electrically conductive. The type of microstructure influenced the conductivity to a larger extent than the $RuO_2$ content. The microstructure of the sinterforged compacts formed from the coprecipitation method led to higher conductivities compared to those from the sequential precipitation method and within the same order of magnitude than for single crystals of $RuO_2$. The ruthenia that segregated into the pores provided excellent continuous pathways for electronic conduction, even at a relatively low $RuO_2$ percentage of 15 mol %. The low percolation limit is believed to derive from the inhomogeneous phase distribution. The more homogeneous distribution of the large $RuO_2$ grains of the compact made from a sequentially precipitated powder led to an electrical conductivity that was lower than those for the coprecipitated compacts. The $RuO_2$ grains in the former were "less connected", forming fewer pathways for electron conduction.

These compacts might be interesting as electrode material due to their high electronic conductivity and their temperature stability. Because of the presence of the stabilizing zirconia phase, sublimation and consequent loss of the ruthenia phase out of the system was greatly inhibited.

**Acknowledgment.** We thank Mr. C. van Dijk and Prof. J. T. M. de Hosson at the Department of Applied Physics at the University of Groningen for the SEM micrographs and gratefully acknowledge the group Chemical Sciences (CW) of the Netherlands Organisation for Scientific Research (NWO) for financial support.

CM001188O